Int. J. Heat Mass Transfer. Vol. 35, No. 10, pp. 2429–2434, 1992
Printed in Great Britain

0017–9310/92 $5.00 + 0.00
Pergamon Press Ltd

An analysis of rivulet formation during flow of an air/water mist across a heated cylinder

M. TRELA and J. MIKIELEWICZ
Institute of Fluid Flow Machines, Polish Academy of Sciences, ul. Gen. Fiszera 14, 80-952 Gdańsk, Poland

(*Received* 6 *August* 1991)

Abstract—Experimental and analytical investigations of rivulet formation on a heated circular cylinder in an air–water mist flow are performed. The primary objective of the experimental part of the research is to obtain data and observations to help formulate and test the analytical model which is based on the small perturbation theory. The effect of approach velocity and mist quality on the rivulet number is examined.

1. INTRODUCTION

ADDING small water droplets into a single-phase gas flow, forms an air–water mist flow, which can enhance the performance of heat transfer from a heated body. It happens because the heat transfer mechanism consists of not only the convection heat transfer of single-phase gas flow but also sensible heat transfer due to temperature rise of the water film formed by the impingement of cold droplets on the heated body, and the evaporation heat transfer from the water film. The range of applications for such an effective cooling method is very wide. Mist-cooled condensers used in thermal cycles to recover waste heat and in the emergency cooling system in a nuclear reactor are only two examples. Heat and mass transfer of mist cooling is an extremely complicated phenomenon depending on temperatures, Reynolds number, the ratio of liquid to gas mass flow, droplet size distribution and many other relevant parameters. In the case of surface temperature below the liquid phase boiling point, the heat transfer augmentation is caused mainly by evaporation of the thin liquid film flowing on the heated surface, which is maintained by continuous impingement of the liquid droplets.

A large number of studies on gas–liquid mist cooling have been published. Most of them are devoted to the heat transfer from the body of different geometries such as plate, cylinder or tube banks. An excellent review of these papers has been done recently by Aihara [1]. These works indicate that the heat transfer augmentation depends directly on the wet area fraction, which is defined as the percentage of the total heat transfer area covered by water. The fraction of surface occupied by water depends primarily on two factors: the mass flux of the impinging droplets and the mechanism of water spreading on the surface. The first factor is connected with the number of droplets and can be easily controlled by the water supply. The mechanism of water spreading on the surface is very complex and has been less explored so far. It depends primarily on the body geometry. For bluff bodies, like cylinder observations of Finlay and McMillan [2], Trela [3] indicates that the front part of a cylinder is easily wetted by liquid film. The state of wetting on its rear part depends on the flow conditions. In some circumstances the liquid film breaks down into rivulets in the region of separation which is located at the apex of the cylinder. The number of rivulets affects the intensity of the heat transfer from the cylinder.

The problem of stability of a liquid film flowing on an even surface (vertical wall, tube, etc.), under the action of gravity or shear stresses, has been the subject of many investigations. There are three different approaches to it: a small perturbation theory model, a rivulet model incorporating a minimum energy requirement and a force balance model. The last two approaches are most frequently used. The results obtained so far of the minimum film thickness calculations are summarized by Bankoff and Tung [4]. In this paper the analysis of rivulet formation on curved surface like circular cylinder is presented. The mechanism of the film rupture in this case differs substantially from the previous one. None of the existing film breakdown theories manages to describe this phenomenon on the curved surface when separation of the boundary layer occurs, a new approach is required. An attempt to clarify this problem is shown below.

2. EXPERIMENTAL APPARATUS

Figure 1 illustrates an outline of the wind tunnel and the spray system, whose details are described in refs. [3, 5]. An air–water droplets mixture was produced by four pneumatic nozzles supplied with water and air at constant 2×10^5 Pa pressure. The nozzles were uniformly mounted in tunnel walls of 0.344×0.395 m^2. The air flow was forced by a fan at a rate measured by an Alcock laminar flow meter placed at the air inlet. A test tube made of copper of diameter $d_c =$ 25 mm, and length $L = 0.15$ m was placed hori-

NOMENCLATURE

a	coefficient [s^{-1}]
A	amplitude [m]
c	complex wave speed, $c_r + ic_i$
C_x	drag coefficient
C	constant
d	diameter [m]
F_a	aerodynamic force [N m^{-1}]
F_i	inertia force [N m^{-1}]
F_σ	surface tension force [N m^{-1}]
g	gravitational acceleration [m s^{-2}]
h	ridge height [m]
k	wave number, $2\pi/\lambda$ [m^{-1}]
L	tube length [m]
$\dot{m}_d$	mass flow rate of droplets [kg s^{-1}]
$\dot{m}_g$	mass flow rate of air [kg s^{-1}]
n	number of rivulets
p	pressure [N m^{-2}]
R	radius of the ridge [m]
t	time [s]
u, v	velocity components in the direction of x, y [m s^{-1}]
$\bar{v}_g$	mean velocity in the tunnel [m s^{-1}]
x, y, z	coordinates
$\bar{w}$	velocity vector [m s^{-1}]
W	complex potential, $W = \phi + i\psi$
w	mist quality, $\dot{m}_d/(\dot{m}_g + \dot{m}_d)$.

Greek symbols

α, ϕ	angles shown in Fig. 2
δ_f	film thickness [m]
ζ	impingement efficiency
η	wave amplitude [m]
θ	contact angle
μ	viscosity [N s m^{-2}]
ρ	density [kg m^{-3}]
σ	surface tension [N m^{-1}]
τ	shear stresses [N m^{-2}]
ϕ	velocity potential
ψ	stream function.

Subscripts

c	critical, cylinder
d	droplet
f	front
g	gas (air)
i	imaginary, inside, interface, inertia
l	liquid
m	mist
o	steady state flow, outside
r	rear
t	tunnel
w	wall
∞	infinity (far upstream).

zontally at the center of the tunnel, at a distance of 4.28 m from the nozzles. The tube, equipped with a cartridge heater inside and four thermocouples placed in its 5 mm thick wall, was axially divided in the vertical plane. Both parts of it were thermally separated by a 2 mm thick laminated epoxy washer coated with copper on two sides. The section of the duct between the spray assembly and the tube was made transparent by using the acrylic plates to enable the visualization of rivulet formation on the tube. Droplet size measurement was carried out using an immersion-sampling method by capturing the droplets on a plate coated with magnesium oxide.

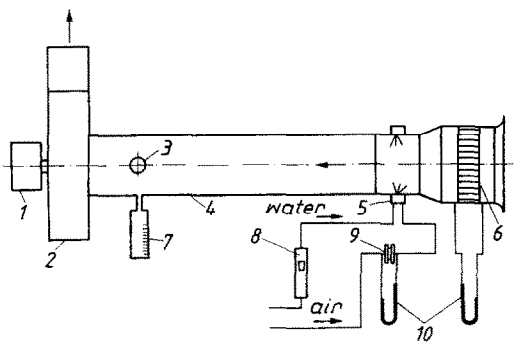

FIG. 1. General arrangement of the test rig. 1 motor, 2 fan, 3 test cylinder, 4 wind tunnel, 5 spray nozzles, 6 air flow meter, 7 collection flask, 8 rotameter, 9 orifice, 10 differential manometers.

The experiments were performed in the following parametric range:

average mist velocity in the tunnel	$\bar{v}_g = 1$–15 m s^{-1},
mist temperature	$T_m = 9$–12°C,
mist quality	$w = 0$–0.02,
Sauter mean diameter of droplets	$d_{32} \simeq 80$ μm,
temperature of the front half of the tube	$T_{wf} \simeq 30$°C,
temperature of the rear half of the tube	$T_{wr} = 30$–50°C,
heat input	$N = 10$–230 W.

3. EXPERIMENTAL DATA

The experimental data obtained indicate that the mechanism of rivulet formation on the cylinder depends mainly on the mist flow velocity. This is depicted schematically in Fig. 2. One may distinguish two general cases due to the mist velocity.

In the low velocity range, Fig. 2(a), the front part of the cylinder is almost covered by a liquid film which forms a wavy unstable ridge at the upper part of it, in the region of the gas boundary layer separation. This ridge produces rivulets which flow downstream on the liquid layer under the action of gravity. There is a lateral flow of water in the ridge. It may be concluded

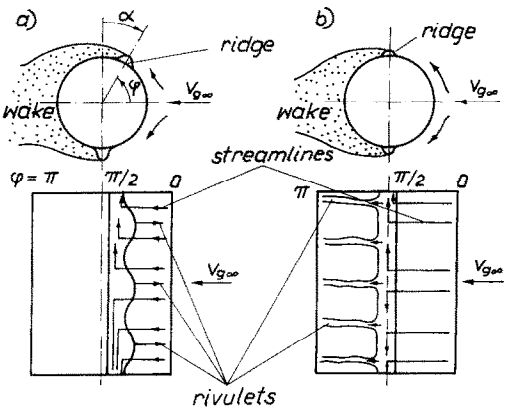

FIG. 2. Liquid flow patterns observed on the circular cylinder: (a) low velocity range, (b) high velocity range.

from the obtained results that this mode of rivulet formation takes place when the mist velocity is less than a certain critical value. In our experiments the critical value was equal to about 6 m s^{-1}.

The increase in the value of the mist velocity forces the separation point and the ridge to move in the direction of the tube apex, Fig. 2(b). For a sufficient droplet supply to the cylinder, the ridge becomes unstable and breaks down to the rivulets which flow on the rear part of the cylinder. A fraction of liquid in the ridge flows in the lateral direction. Figure 3 presents experimental data obtained for the higher range of the mist velocities. The number of rivulets flowing on the downward part of the cylinder is plotted against the quality and velocity of the mist flow.

4. PHYSICAL MODEL AND THEORETICAL ANALYSIS

Theoretical analysis of the rivulets formation on the cylinder is based primarily on three conclusions which can be drawn from the obtained results and observations made during the experiments.

First, for both modes of rivulet formation, i.e. at low and high mist velocities, the rivulets originate from the unstable ridge which is located at a separation point of the cylinder. Second, the liquid flow in the ridge resembles a flow in the neighborhood of a stagnation point. Third, the formation of rivulets is preceded by an appearance of irregularities at the ridge free interface, which are amplified in the course of time.

The analysis will be performed for the high and the low velocity ranges of the mist flow.

High velocity range

Let us consider a circular cylinder flowed over by a mist flow at the high velocity range. The liquid ridge is built up at the apex of the cylinder, as shown in Fig. 2(b) and Fig. 4.

The following assumptions are made for simplification:

(1) Water film flow along the forward part of the cylinder is laminar.

(2) The boundary layer over the water film is laminar.

(3) Reflection of droplets from the film surface does not occur.

(4) The concentration of droplets is relatively low, so the influence of depositing droplets on the boundary layer parameters can be neglected.

(5) The flow of water in the ridge is treated as a frictionless potential flow in the vicinity of a stagnation point.

(6) The cross-sectional shape of a circular segment is assumed for the ridge, Fig. 4.

(7) The instability of the ridge in its early stage can be described by the method of small perturbation theory.

The velocity distribution in frictionless potential flow in the neighborhood of a stagnation point may be described by the complex potential W, which has the form

$$W = \frac{az^2}{2} = \frac{a}{2}[(x^2 - y^2) + i2xy] \tag{1}$$

where $z = x + iy$, is the complex variable.

The velocity components, u_o, v_o of the vector $\bar{w}$ (u_o, v_o) can, therefore, be expressed as

$$u_o = \frac{\partial \phi_o}{\partial x} = ax; \quad v_o = \frac{\partial \phi_o}{\partial y} = -ay. \tag{2}$$

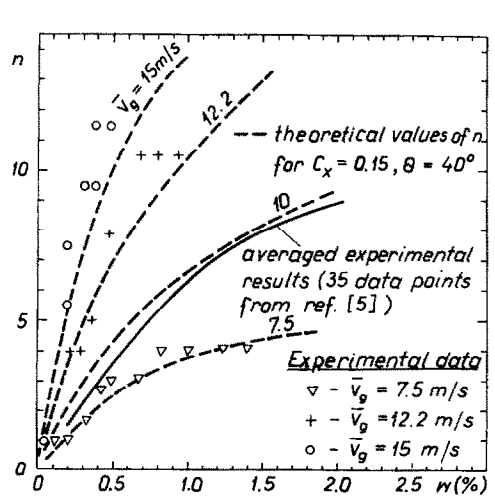

FIG. 3. Comparison between theoretical and experimental values of the rivulet number.

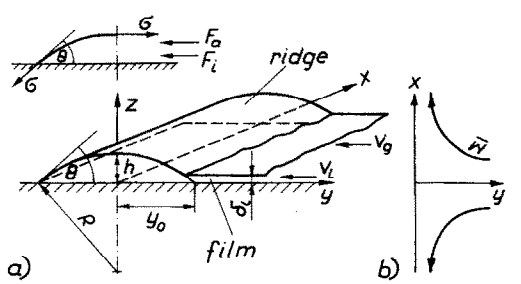

FIG. 4. Physical model: (a) ridge configuration, (b) liquid path.

The solution of Euler momentum equation for inviscid flow

$$\rho\frac{\mathrm{D}\bar{w}}{\mathrm{D}t}=\rho\bar{g}-\nabla p_{\mathrm{i}} \tag{3}$$

is given by

$$p_{\mathrm{i}}-p_{\mathrm{o}}=-\rho\left(\frac{\partial\phi_{\mathrm{o}}}{\partial t}+\frac{w^2}{2}+gz\right). \tag{4}$$

If the flow is steady and the influence of gravity may be neglected, as in the considered case, then the first and the third terms in the bracket can be omitted.

To describe the flow in the ridge, one must determine the coefficient a in equation (1). This may be done with the use of a force balance equation which is applied to the ridge, Fig. 4. For the stable equilibrium of the ridge, the surface tension force F_σ balances the fluid pressure owing to the change of flow direction and the aerodynamic force F_{a} exerted by the mist flow on the ridge, thus the following relation holds:

$$C_{\mathrm{x}}(h-\delta_{\mathrm{l}})\rho_{\mathrm{g}}\frac{v_{\mathrm{g}}^2}{2}+\rho_{\mathrm{l}}v_{\mathrm{l}}^2\delta_{\mathrm{l}}=\sigma(1-\cos\theta). \tag{5}$$

Taking into account equation (2) and Fig. 4, the velocity component v_{l} becomes

$$v_{\mathrm{l}}=v_{\mathrm{o}}|_{y=y_{\mathrm{o}}}=-ay_{\mathrm{o}}=-aR\sin\theta. \tag{6}$$

If we define a coefficient B as

$$B=\frac{C_{\mathrm{x}}\delta_{\mathrm{l}}\rho_{\mathrm{g}}v_{\mathrm{g}}^2}{2(1-\cos\theta)} \tag{7}$$

and make use of the geometrical relation $h=R(1-\cos\theta)$, then according to equation (5)

$$a=-\frac{C_{\mathrm{x}}v_{\mathrm{l}}\rho_{\mathrm{g}}v_{\mathrm{g}}^2}{2\left(\sigma+B-\dfrac{\rho_{\mathrm{l}}v_{\mathrm{l}}^2\delta_{\mathrm{l}}}{1-\cos\theta}\right)\sin\theta}. \tag{8}$$

The details of evaluation of velocities v_{l}, v_{g} and other relevant parameters are given in the Appendix.

Now let us impose small disturbances on the primary flow which was assumed to be steady and irrotational. The flow due to the disturbances is also irrotational. The velocity potential ϕ, velocity $\bar{w}$ and the pressure drop Δp_{i} can be written as

$$\phi=\phi_{\mathrm{o}}+\phi' \tag{9}$$

$$\bar{w}=\bar{w}_{\mathrm{o}}+\bar{w}'=i(u_{\mathrm{o}}+u')+j(v_{\mathrm{o}}+v') \tag{10}$$

$$\Delta p_{\mathrm{i}}=\Delta p_{\mathrm{io}}+\Delta p_{\mathrm{i}}'. \tag{11}$$

The superimposed fluctuating velocity $\bar{w}'$ is assumed small in the sense that all quadratic terms of its components may be neglected with respect to the linear terms, thus we have

$$\bar{w}^2=u_{\mathrm{o}}^2+2u_{\mathrm{o}}u'+2v_{\mathrm{o}}v'+v_{\mathrm{o}}^2. \tag{12}$$

Substitution of equation (12) into equation (4) and neglecting the gravity term yields

$$\Delta p_{\mathrm{i}}'=-\rho_{\mathrm{l}}\left(\frac{\partial\phi}{\partial t}+u_{\mathrm{o}}u'+v_{\mathrm{o}}v'\right). \tag{13}$$

The disturbance of the pressure leads to the displacement η of the ridge free interface, which is assumed to be periodic in x, thus we consider the displacement η to have the form

$$\eta=A\exp[ik(x-ct)]. \tag{14}$$

The fluid velocity fluctuation v' on the ridge interface can be written as

$$v'=\frac{\mathrm{D}\eta}{\mathrm{D}t}=\frac{\partial\eta}{\partial t}+u_{\mathrm{o}}\frac{\partial\eta}{\partial x}\simeq\frac{\partial\eta}{\partial t} \tag{15}$$

according to the assumption of the small disturbances theory. Since the imposed flow was assumed to be irrotational then velocities u' and v' can be expressed by potential ϕ

$$u'=\frac{\partial\phi}{\partial x};\quad v'=\frac{\partial\phi}{\partial y} \tag{16}$$

which satisfies the Laplace equation

$$\frac{\partial^2\phi}{\partial x^2}+\frac{\partial^2\phi}{\partial y^2}=0. \tag{17}$$

Comparison of equation (15) with equation (16) provides the relation

$$\frac{\partial\phi}{\partial y}=\frac{\partial\eta}{\partial t} \tag{18}$$

which is the kinematic condition at the free interface.

The solution of the Laplace equation (17) depends on the nature of the boundary conditions. It was shown in ref. [10] that for surface waves of small amplitude generated either in a semi-infinite liquid or in the liquid layer of finite depth, the depth is quite unimportant, therefore in order to simplify the problem we seek the solution of equation (17) in the form

$$\phi=C\exp(-ky)\exp[ik(x-ct)] \tag{19}$$

which is obtained by imposing the boundary condition on equation (17) that $v'\Rightarrow 0$ for $y\Rightarrow\infty$. The disturbance of the pressure at the free interface is balanced by the surface tension force, thus

$$\Delta p_{\mathrm{i}}'=\sigma\left(\frac{1}{R_{yx}}+\frac{1}{R_{yz}}\right) \tag{20}$$

where R_{yx} and R_{yz} are the two principal radii of curvature at the ridge free interface,

$$\frac{1}{R_{yx}}=-\frac{\partial^2\eta/\partial x^2}{[1+(\partial\eta/\partial x)^2]^{3/2}}\simeq-\frac{\partial^2\eta}{\partial x^2} \tag{21}$$

$$\frac{1}{R_{yz}}\simeq\frac{\eta}{R^2}. \tag{22}$$

Taking into account equations (20) to (22) and (13), the dynamic condition at the free ridge interface can be formulated:

$$-\rho_l\left(\frac{\partial\phi}{\partial t}+u_o\frac{\partial\phi}{\partial x}\right)=\sigma\left(-\frac{\partial^2\eta}{\partial x^2}+\frac{\eta}{R^2}\right). \quad (23)$$

In equation (13) the term $y_o v'$ was neglected since for $y=0$, $v_o=0$. With the use of equations (14), (18), (19) one gets from the above equation the relation for the complex wave velocity

$$c^2-u_o c+\frac{\sigma}{\rho_l k}\left(k^2+\frac{1}{R^2}\right)=0. \quad (24)$$

If only the wave motion is considered on the distance equal to the wavelength λ, i.e. if $x=\lambda=2\pi/k$ and $u_o=a2\pi/k$, then the solution of the above equation takes the form

$$c_{1,2}=\frac{\pi}{a}\pm\left[\left(\frac{\pi a}{k}\right)^2-\frac{\sigma}{\rho_l k}\left(k^2+\frac{1}{R^2}\right)\right]^{1/2}. \quad (25)$$

Inspection of equation (14) reveals that the disturbance will grow if c_i is positive and be damped if c_i is negative. In the limit when $c_i=0$ one gets the equation for the critical wavenumber k_c from equation (25)

$$k_c^3+\frac{k_c}{R^2}-\frac{\pi^2 a^2\rho_l}{\sigma}=0. \quad (26)$$

The solution of this equation is given by

$$k_c=-Q^{1/3}\{[1-(1+m)^{1/2}]^{1/3}+[1+(1+m)^{1/2}]^{1/3}\} \quad (27)$$

where

$$m=P^3/Q^2;\quad P=1/(3R^2);\quad Q=-\pi^2 a^2\rho_l/2\sigma. \quad (28)$$

The number of rivulets on the cylinder can thus easily be evaluated since the rivulet pitch equals the wavelength λ

$$n=\frac{L}{\lambda}=L\frac{k_c}{2\pi}. \quad (29)$$

Figure 3 shows comparison of experimental data for the rivulet number n with the foregoing theory. In the calculation, the values of drag coefficient C_x and the contact angle θ were assumed. The first quantity was taken to be $C_x=0.15$ supposing the ridge aerodynamic characteristic is similar to a streamlined cylinder.

Determination of the dynamic contact angle is a very complex problem. Recent investigations by Trela [5] and Hirasawa and Hauptmann [11] suggest that this factor may not be considered as a physical property, but the dependent quantity which is still an unknown function of many variables such as liquid flow rate, surface properties and heat flux, thus the value of contact angle $\theta=40°$ was taken from observation. The assumptions concerning C_x and θ are admittedly crude, nevertheless these are considered the only practical way of performing the calculations of the rivulet number.

It is seen by inspection of Fig. 3 that increase in value for both velocity and mist quality favors the wetting of the rare part of the tube. The agreement between the experimental and calculated values of the rivulets number n is quite satisfactorily for such complex phenomenon.

Low velocity range

In the low velocity range the rivulets flow down on the forward part of the cylinder. It was found that for this case the ridge instability is of the Taylor type. Taylor instability occurs when a heavier fluid is on top of a lighter fluid [6]. The instability wave most likely to appear at the interface has a wavelength

$$\lambda=2\pi\left(\frac{3\sigma}{(\rho_l-\rho_g)g\sin\alpha}\right)^{1/2} \quad (30)$$

where α is the angle shown in Fig. 2.

The rivulet number n for this case is equal to

$$n=\frac{L}{2\pi}\left(\frac{(\rho_l-\rho_g)g\sin\alpha}{3\sigma}\right)^{1/2}. \quad (31)$$

During the experiments carried out in the range of mist quality $w=0.8$ to 1.5% it was found by Trela [3] that 3 to 4 rivulets were generated on the cylinder at the value of the angle $\alpha\simeq 30°$. This is in agreement with the above formula which provides $n=3.5$ in such case. The observations indicate that increase in quality forces the angle α to rise. At its limiting value of 90° equation (31) provides $n=5$. This is in agreement with observations of the phenomenon, which revealed the appearance of about 4 to 5 rivulets at the highest mist quality ($\simeq 2\%$).

5. CONCLUSIONS

The problem of rivulet formation on a circular horizontal cylinder flowed over by an air–water mist is discussed. The results obtained lead to the following conclusions.

(1) There are two modes of rivulet formation: at high and low values of the mist velocities.

(2) For the high velocity the process can be analyzed with the use of modified small disturbance theory and two additional principal assumptions concerning the flow distribution in the ridge and the condition for the stable equilibrium of it in the steady state. There are two parameters introduced into the theory: drag coefficient C_x and contact angle θ. The comparison of the experimental data with the numerical results suggest, to a first approximation, the values of these parameters to be $C_x=0.15$ and $\theta=40°$.

(3) In the low velocity range, rivulet formation is governed by the Taylor instability. The only parameter here is an angle of the ridge inclination α, which is an unknown function of velocity and quality of the mist. As far as the process of a surface wetting is considered, this case of rivulets formation is of less importance for heat transfer, since the rivulets flow down on the liquid layer.

It should be noted that the analysis does not include the effect of heat flux. For the conditions of the experiments the values of the heat flux were relatively low, so this influence may be omitted.

REFERENCES

1. T. Aihara, Augmentation of convective heat transfer by gas–liquid mist, *Proc. Int. Heat Transfer Conf.*, Jerusalem, Vol. 1, pp. 445–461 (1990).
2. I. C. Finlay and T. McMillan, Heat transfer during two-component mist flow across a heated cylinder, *Proc. Instn Mech. Engr* **182,** 3H, 277–288 (1967–1968).
3. M. Trela, Heat and mass transfer during mist flow (in Polish), Report of IFFM 154/1069/83 (1983).
4. S. G. Bankoff and H. Tung, Rivulet formation on a heated wall, *Proc. Int. Heat Transfer Conf.*, Munich, pp. 363–367 (1982).
5. M. Trela, Some hydrodynamics problems of liquid behavior on the wall in two-phase dispersed flow (in Polish), Report of IFFM 293/1214/89 (1989).
6. D. Yung, J. J. Lorenz and E. N. Ganić, Vapor/liquid interaction and entrainment in falling film evaporators, *Trans. ASME, J. Heat Transfer* **102,** 20–25 (1980).
7. J. G. Knudsen and D. L. Katz, *Fluid Dynamic and Heat Transfer*. McGraw Hill, New York (1958).
8. H. Schlichting, *Boundary Layer Theory*. McGraw Hill, New York (1955).
9. A. Žukauskas, *Advances in Heat Transfer* (Edited by J. M. Hartnett and T. F. Irvine), Vol. 8, pp. 93–160. Academic, New York (1972).
10. C. S. Yih, *Fluid Mechanics*. McGraw Hill, New York (1969).
11. S. Hirasawa and E. G. Hauptmann, Dynamic contact angle of a rivulet flowing down a vertical heated wall, *Proc. Int. Heat Transfer Conf.*, San Francisco, Vol. 4, pp. 1877–1882 (1986).

APPENDIX

Mass flow rate of droplets $\dot{m}_{dc}$ deposited on the forward part of the cylinder is given by

$$\dot{m}_{dc} = \zeta w L d_c \bar{v}_g \rho_g. \tag{A1}$$

The impingement efficiency ζ was calculated using the formula [3]

$$\zeta = \frac{Stk^3}{Stk^3 + 0.77Stk^2 + 0.22} \tag{A2}$$

where

$$Stk = \frac{\rho_l d_d^2 v_{g\infty}}{18\mu_g d_c} \quad \text{Stokes number.}$$

Mist velocity approaching the cylinder was treated as the velocity at the tunnel axis. The ratio of average to the maximum velocity in a tunnel can be expressed by an interpolation formula [7]

$$\frac{\bar{v}}{v_{max}} = 0.8 + \frac{\ln(Re_t \times 10^{-4})}{65.51} \tag{A3}$$

where $Re_t = v_{max} d_t \rho_g / \mu_g$ Reynolds number of the tunnel, d_t equivalent tunnel diameter, $d_t = 0.365$ m, $v_{max} = v_{g\infty}$.

Film thickness at the entrance to the ridge is given by

$$\delta_l = \left(\frac{\dot{m}_{dc}\mu_l}{\tau_i \rho_l L}\right)^{1/2}. \tag{A4}$$

Average film velocity v_l is equal to

$$v_l = \frac{\dot{m}_{dc}}{2\rho_l \delta_l L}. \tag{A5}$$

The evaluation of the shear stresses τ_i was based on the boundary layer theory [8] (p. 215, Fig. 12.8) which for the flow past a circular cylinder provides for $\phi = \pi/2$ the relation

$$\tau_i = 1.98 \frac{\rho_g v_{g\infty}^2}{(Re_c)^{1/2}}. \tag{A6}$$

In order to determine the drag force exerted on the ridge the mist velocity v_g has to be known. A velocity distribution outside the boundary layer on the circular cylinder is given by Žukauskas [9]

$$\frac{v}{v_\infty} = 3.63(y/d_c) - 2.171(y/d_c)^3 - 1.514(y/d_c)^5. \tag{A7}$$

For the angle $\phi = \pi/2$, $y = \pi d_c/4$ and the above equation yields

$$\frac{v_g}{v_{g\infty}} = 1.3475. \tag{A8}$$

ANALYSE DE LA FORMATION DE RIGOLES PENDANT L'ECOULEMENT D'UNE BRUME AIR/EAU SUR UN CYLINDRE CHAUFFE

Résumé—On étudie expérimentalement et analytiquement la formation de rigoles sur un cylindre circulaire chauffé dans un écoulement de brume air–eau. L'objectif principal de la partie expérimentale est d'obtenir des données et des observations pour aider la formulation et la validation d'un modèle analytique basé sur la théorie des petites perturbations. On examine l'effet de la vitesse d'approche et la qualité de la brume sur le nombre de rigoles.

ANALYSE DER RINNSALBILDUNG BEI DER STRÖMUNG EINES LUFT/WASSER-NEBELS ÜBER EINEM BEHEIZTEN ZYLINDER

Zusammenfassung—Es werden experimentelle und analytische Untersuchungen zur Rinnsalbildung an einem keilförmigen Zylinder in der Strömung eines Luft/Wasser-Nebels durchgeführt. Das wesentliche Ziel des experimentellen Teils der Untersuchung ist die Ermittlung von Daten und Beobachtungen zur Unterstützung der Formulierung und Validierung des analytischen Modells, das auf der Theorie kleiner Störungen basiert. Der Einfluß der Anströmgeschwindigkeit und der Zusammensetzung des Nebels auf die Anzahl der Rinnsale wird untersucht.

АНАЛИЗ ОБРАЗОВАНИЯ РУЧЕЙКОВ ПРИ ОБТЕКАНИИ ТУМАНОМ НАГРЕТОГО ЦИЛИНДРА

Аннотация—Экспериментально и анагитически исследуется образование ручейков на нагретом круговом цилиндре, обтекаемом туманом. Основной целью экспериментальной части исследования является получение данных для формулировки и проверки аналитической модели, основанной на теории малых возмущений. Рассматривается влияние скорости течения и характеристик тумана на количество ручейков.